AIAA 2006-2165

Variable Stiffness Panel Structural Analyses with Material Nonlinearity and Correlation with Tests

K. Chauncey Wu
NASA Langley Research Center
Hampton, Virginia

Zafer Gürdal
Delft University of Technology
Delft, The Netherlands

47th AIAA/ASME/ASCE/AHS/ASC Structures, Structural Dynamics and Materials Conference
1-4 May 2006
Newport, Rhode Island

Variable Stiffness Panel Structural Analyses with Material Nonlinearity and Correlation with Tests

K. Chauncey Wu*
NASA Langley Research Center
Hampton, Virginia 23681-2199
and
Zafer Gürdal†
Delft University of Technology
Delft, The Netherlands

Abstract

Results from structural analyses of three tow-placed AS4/977-3 composite panels with both geometric and material nonlinearities are presented. Two of the panels have variable stiffness layups where the fiber orientation angle varies as a continuous function of location on the panel planform. One variable stiffness panel has overlapping tow bands of varying thickness, while the other has a theoretically uniform thickness. The third panel has a conventional uniform-thickness $[\pm 45]_{5S}$ layup with straight fibers, providing a baseline for comparing the performance of the variable stiffness panels. Parametric finite element analyses including nonlinear material shear are first compared with material characterization test results for two orthotropic layups. This nonlinear material model is incorporated into structural analysis models of the variable stiffness and baseline panels with applied end shortenings. Measured geometric imperfections and mechanical prestresses, generated by forcing the variable stiffness panels from their cured anticlastic shapes into their flatter test configurations, are also modeled. Results of these structural analyses are then compared to the measured panel structural response. Good correlation is observed between the analysis results and displacement test data throughout deep postbuckling up to global failure, suggesting that nonlinear material behavior is an important component of the actual panel structural response.

Introduction

The widespread use of polymer composite materials in aerospace vehicle structures has stimulated concurrent development of sophisticated manufacturing technology for their fabrication. The introduction of commercial systems for precise, repeatable placement of preimpregnated (prepreg) composite tows marks a significant advancement in composite fabrication technology. One such advanced tow (or fiber) placement system is Cincinnati Machine's Viper FPS-3000 Fiber Placement System¶ (Ref. 1). Advanced tow placement systems like the Viper FPS are enabling technology which permit efficient fabrication of advanced composite structures, defined here as structures where the fibers within a given ply may be laid down following complex, curvilinear paths. The fiber orientation angle in advanced composite structures

---

* Aerospace Engineer, Vehicle Analysis Branch, SACD. 1 North Dryden Street, Mail Stop 451. k.c.wu@nasa.gov
† Chair, Faculty of Aerospace Structures. Kluyverweg 1, 2629 HS Delft. Associate Fellow, AIAA. z.gurdal@lr.tudelft.nl

¶ Identification of commercial products and companies in this paper is used to describe the materials adequately. The identification of these commercial products does not constitute endorsement, expressed or implied, of such products by the National Aeronautics and Space Administration.

varies continuously both within each ply and throughout the structure, and fibers are not required to be straight and parallel in each ply (as is the case for conventional composites). These advanced configurations are often referred to as "variable stiffness" structures, since the laminate stiffnesses also vary continuously across the structure planform.

Analyses performed in Refs. 2 and 3 suggest that variable stiffness panels subjected to in-plane loads can be tailored to have much higher buckling resistance than equal-weight, conventional angle-ply laminates made of the same materials. The structural response of variable stiffness panels with a manufacturing constraint on fiber radius of curvature is evaluated in Ref. 4. The in-plane response of symmetrically laminated variable stiffness laminates with regions of overlapping tow bands (generated by placement of adjacent tows during the manufacturing process) is evaluated in Ref. 5. The overlapping tow bands form local areas of increased thickness on the laminate that resemble discrete stiffeners, and are more complicated to analyze than the constant-thickness laminates studied previously.

A convention for the definition of tow paths for rectangular variable stiffness panels, introduced in Ref. 2, is used here. A reference tow path (shown as a bold line in Figure 1) is first defined which passes through the panel geometric center. The fiber orientation angle of this tow path varies linearly over a specified distance, measured from the panel center, in both directions along the Y-axis. The fiber orientation angle Θ for the reference tow path varies from 60 degrees along the panel axial centerline to 30 degrees along the panel edges 12 inches away. The additional tow paths shown in the figure are generated by replicating the reference tow path in uniform increments in both directions along the panel X-axis (±3.464 inches here), forming the complete variable stiffness ply.

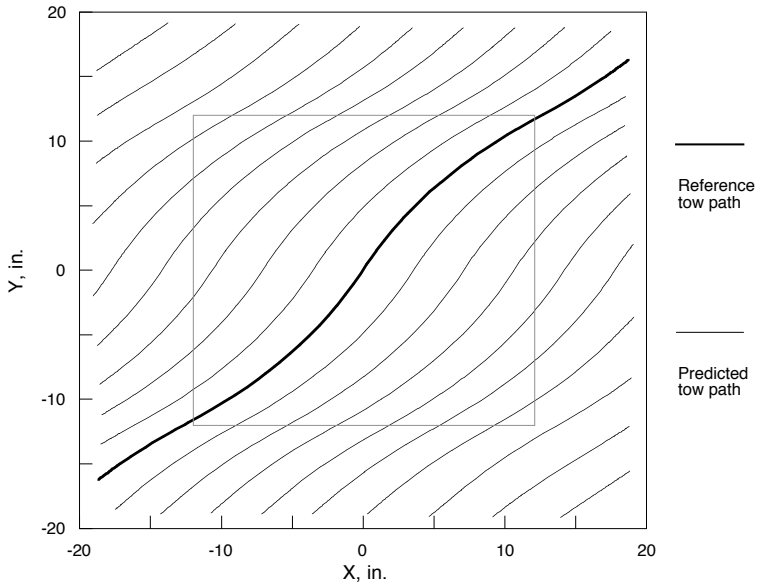

Figure 1. Variable stiffness ply tow path centerlines

The selection of one variable stiffness panel design for further study is presented in Ref. 6, along with fabrication details for two first-generation panels made from AS4/977-3 prepreg tows. While both variable stiffness panels have the same nominal $[\pm 45/(\pm\Theta)_4]_S$ layup, one panel has overlapping tow bands of varying thickness (see Figure 2), and is thus designated as the *panel with overlaps*. This asymmetric panel differs from the structures described in Ref. 5 in that it is laid up on a flat tool surface, so all of the overlaps are located on one side of the panel. The second variable stiffness panel uses the tow drop/add capability of the tow placement system to generate a theoretically uniform thickness panel, denoted as the *panel without overlaps*. A third conventional panel with a uniform thickness, straight fiber $[\pm 45]_{5S}$

layup is fabricated using the same materials and processes, and serves as the baseline for comparison with the variable stiffness panel performance.

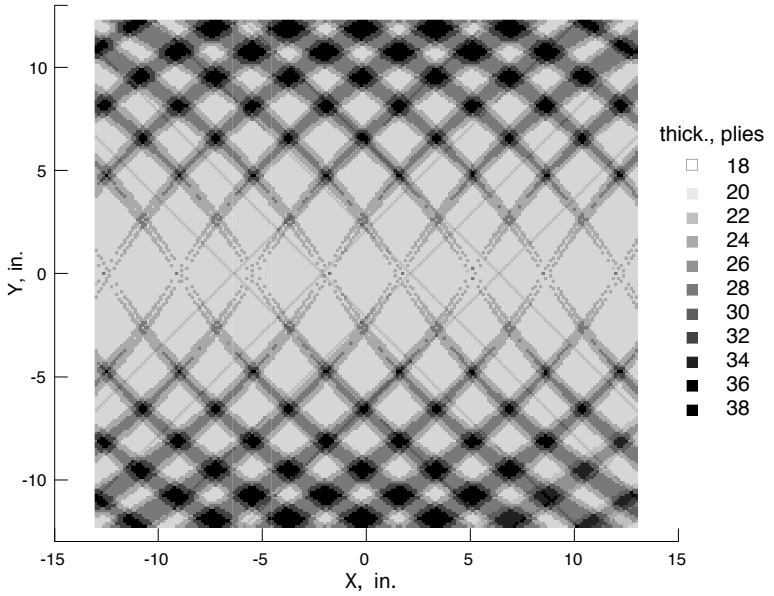

Figure 2. Predicted laminate thickness for panel with overlaps

Additional fabrication issues for these variable stiffness panels are presented and discussed in Ref. 7, along with a comparison of measured and predicted laminate coefficients of thermal expansion. A follow-on study in Ref. 8 presents selected results from experiments performed to determine the structural response of the variable stiffness and baseline panels under mechanical end shortening loads. Test results are also compared therein with results from geometrically nonlinear structural analyses of the variable stiffness panels with linear material behavior and both mechanical and thermal prestresses. Excellent correlation is also observed between measured and predicted results for the baseline panel for applied loads up to 8 klb.

Measured deflections and strains presented in Ref. 8 for the panel with overlaps agree well in the prebuckling load range and near buckling with results from an analysis including mechanical prestresses. These mechanical prestresses are generated by forcing the variable stiffness panels from their anticlastic cured shape into their flattened test configuration in test fixtures. The poor correlation for the panel without overlaps with mechanical prestresses in that study is believed to result from an error in the imperfection model of the fixtured panel. The correlation in the deep postbuckling load regime becomes worse as the loads and deflections increase, suggesting that the linear material model used in those analyses may not be fully adequate for predicting the panel structural response.

Compression tests of angle-ply coupons reported in Ref. 9 show that fiber-dominated laminate stress-strain relationships are typically linear, whereas laminates that carry loads in matrix shear have nonlinear relationships. Since the variable stiffness and baseline panels in Refs. 7 and 8 have layups with fiber orientation angles that vary between 30 and 60 degrees, nonlinear matrix shear behavior is thought to have a significant effect on the panel structural response. Better correlation of analytical and measured results may be possible if a nonlinear material model is used in conjunction with the geometrically nonlinear structural analyses. The objectives of the present study are to model the structural response of material characterization coupons and the variable stiffness and baseline panels including material nonlinearities. This study is therefore an extension of Ref. 8, where results of structural analyses of the variable stiffness and baseline panels with only geometric nonlinearities are presented.

To achieve this goal, a simple material model that includes nonlinear material shear is first introduced. Parametric structural analyses including this nonlinear shear response are performed and compared with results of material characterization tests for two orthotropic laminates. This nonlinear material model is then incorporated into finite element models of the variable stiffness and baseline panels. Measured geometric imperfections and mechanical prestresses from the panel fixturing process are also modeled. Results of these structural analyses including both geometric and material nonlinearities are presented and compared with test data for the variable stiffness panels presented in Ref. 8.

Nonlinear material model and characterization

A nonlinear elastic material model for a composite ply developed by Hahn and Tsai (Ref. 10) is implemented in the STAGS nonlinear shell analysis code (Ref. 11). The ply longitudinal and transverse stress-strain responses in this model are both linear-elastic, while the in-plane shear strain is modeled as a nonlinear-elastic, cubic function of the shear stress,

$$\gamma_{12} = G_{12}^{-1}\tau_{12} + S_{6666}\,\tau_{12}^{3} \qquad (1).$$

The nonlinear shear coefficient S_{6666} has units of $(lb/in^2)^{-3}$ and is associated with the nonlinear shear stress term in Equation 1.

Short-block material characterization tests (Ref. 9) are performed on $[0/90]_{5s}$ and $[\pm45]_{5s}$ coupons. These test specimens, fabricated from AS4/977-3 graphite/epoxy prepreg, are cut from scrap material surrounding the baseline panel. Linear material properties for an AS4/977-3 composite ply (E_1 = 18.83 Mlb/in^2, E_2 = 1.34 Mlb/in^2, ν_{12} = 0.36 and G_{12} = 0.74 Mlb/in^2), first reported in Ref. 7, are estimated from inverse solutions using these orthotropic laminate test data since uniaxial laminates were not available for testing. Structural analyses of these two cross-ply laminates including geometric and material nonlinearities are performed and compared with test results. This comparison serves to determine the validity of these nominal material properties, and also to estimate appropriate values of the nonlinear shear coefficient S_{6666} for use in structural analyses of the variable stiffness and baseline panels.

Coupons with dimensions of 1.75 x 0.75 inches are instrumented with axial and transverse strain gages located at the specimen center. Experimentally determined axial stresses for a representative test of a $[\pm45]_{5s}$ laminate are plotted against the measured strains in Figure 3. The high degree of material nonlinearity in this laminate is evident from the experimental results. A STAGS finite element model of the material characterization test is then developed to predict the laminate response for integer values of S_{6666}. The thin solid lines labeled S_{6666} = 0 in Figure 3 are the results for a linear material model, and show good correlation with the measured data up to about 10 klb/in^2. Although they are modeled, no geometric nonlinearities are noted in the responses. Predicted stress-strain curves for several nonzero values of S_{6666} are also shown in the figure as dashed lines, with the test data bounded by values of S_{6666} between 0 and 2 x 10^{-14} $(lb/in^2)^{-3}$.

The short-block compression test is also used to evaluate the axial and transverse strain response of a $[0/90]_{5s}$ laminate in which minimal matrix shearing is expected. Measured axial stresses for this laminate are plotted against the axial and transverse strains in Figure 4, with the transverse strain data multiplied by a factor of ten for clarity. The strain responses of this laminate to the applied end shortening are mildly nonlinear over the range of stresses plotted in the figure. The measured nonlinear behavior shown in the figure is most likely due to the nonlinear transverse stiffness E_2 of the composite ply, since the theoretical shear strains are zero for this laminate.

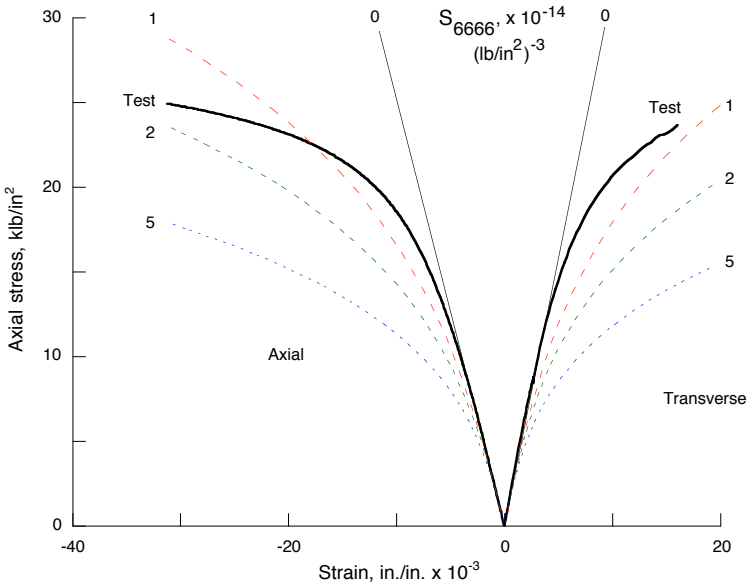

Figure 3. Axial stress vs. strain for $[\pm 45]_{5S}$ laminate

The analysis model of the short-block test is then modified to represent the $[0/90]_{5S}$ laminate, and the linear response for $S_{6666} = 0$ is plotted against the test results in Figure 4. The predicted axial strain response from this analysis with linear material properties compares well with the test data at applied stresses up to 15 klb/in^2, while the transverse strains agree well up to 50 klb/in^2. Analytical results are also generated for several nonzero values of S_{6666}, but are not shown because they are identical to the results for $S_{6666} = 0$.

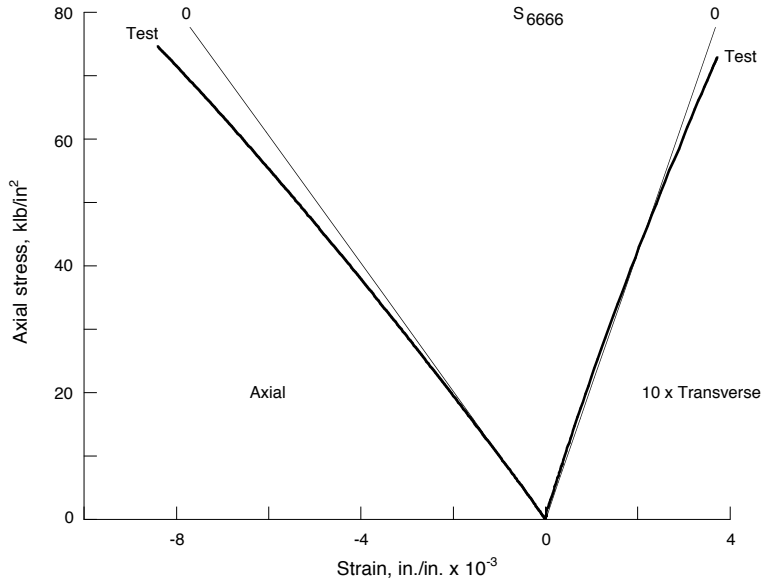

Figure 4. Axial stress vs. strain for $[0/90]_{5S}$ laminate

The correlation shown in these figures indicates that the linear ply material properties, computed from laminate test data using inverse methods, are reasonable for predicting the initial structural response. No single value of the nonlinear shear coefficient S_{6666} provides good correlation across the entire range of test data for the two laminates studied here. *However, the test data are all well bounded by results from the analyses with* $S_{6666} = 0$ *and* 2×10^{-14} $(lb/in^2)^{-3}$. Therefore, the nonlinear shear coefficient S_{6666} will be treated as a parametric term in the following analyses of the variable stiffness and baseline panels.

Panel with overlaps

Structural models of the variable stiffness panels that include the nonlinear material response are generated using the STAGS analysis code. The finite element mesh for these 26 x 24.5-inch panels has 1520 elements and 1599 nodes, with additional mesh refinement provided around the strain gage locations on the panel axial and transverse centerlines. Each finite element in the panel with overlaps model has a unique layup and thickness. The laminate thicknesses assigned are shown in Figure 5, and range from 20 to 36 plies (0.153 to 0.275 inches). While the level of refinement in this model is obviously not as great as that shown in Figure 2, the tow overlaps and variable stiffness tow patterns are still evident. Fiber orientation angles for the first variable stiffness ply of this model are illustrated in Figure 6, with the discretization again apparent.

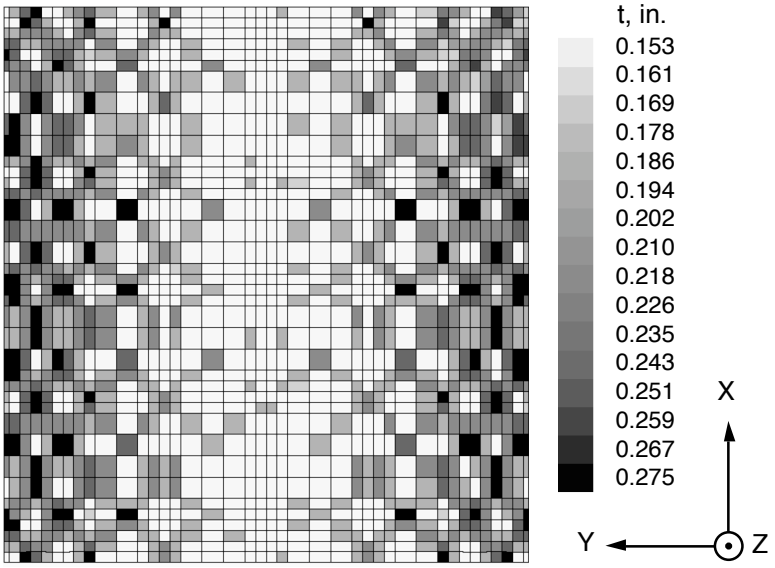

Figure 5. Predicted laminate thickness for panel with overlaps analysis model

Measured geometric imperfections for the panel with overlaps without and with test fixtures are presented in Refs. 7 and 8. Large imperfections in the unfixtured, cured variable stiffness panels required development of special test fixtures to flatten these panels during test preparation. The resulting mechanical prestresses are modeled in the finite element analyses by using applied normal displacements to gradually flatten the variable stiffness panels from their anticlastic cured shapes into their tested configurations. Boundary conditions representing the restraints of the attached structural test fixtures are specified on the panel edges, then the applied end shortening is simulated by applying a uniform axial displacement along the panel's upper edge.

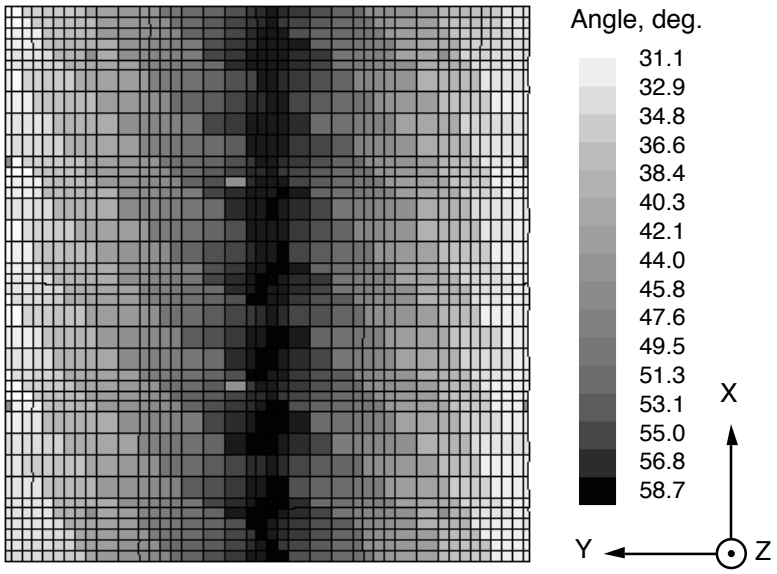

Figure 6. Fiber orientation angles for panel with overlaps analysis model

Axial and normal deflections

The predicted compressive load for the panel with overlaps subjected to applied end shortenings of up to 0.130 inches (the maximum measured value) is presented in Figure 7. The results of these geometrically nonlinear analyses include the effects of the mechanical prestresses as well as the nonlinear material model described above. Of the five curves in the figure, the curve labeled $S_{6666} = 0$ is identical to the results with the linear material model presented in Ref. 8. The predicted axial load is plotted against the end shortening for three integer values of S_{6666} to demonstrate the sensitivity of the predicted response to increasing degrees of material nonlinearity. The measured panel response is also shown on the plot as a thick solid line. The initial nonlinearity in the test set-up all occurs below 1500 lb load. Between the end shortenings corresponding to that load and panel failure, *predicted axial loads from an analysis with* $S_{6666} = 4 \times 10^{-14}$ *(lb/in*^{2}*)*$^{-3}$ *compare very well with the test data*, with a root-mean-square (RMS) difference of 2.2 percent.

The prebuckling axial stiffness K_o and the transition load P_{tr} (defined in Ref. 8 as the load when the linear prebuckling load-end shortening curve first becomes nonlinear) are computed from the load-end shortening curve with $S_{6666} = 4 \times 10^{-14}$ (lb/in^2)$^{-3}$ and reported in Table 1. The predicted prebuckling stiffness of 664.30 klb/in. is within 2.2 percent of the measured panel stiffness, and the transition load from this analysis is 12.39 klb, a 9.6 percent difference from the test result. The predicted axial load on the panel is 42.89 klb at the 0.130-inch maximum applied end shortening, or a 4.3 percent difference from the measured panel failure load of 41.07 klb.

Measured and predicted panel center normal deflections for the panel with overlaps are plotted against the axial load in Figure 8. Only analysis results for $S_{6666} = 0$ and 4×10^{-14} (lb/in^2)$^{-3}$ are presented here for clarity. These normal deflections are defined as positive along the –Z-axis, since the panel center moves in that direction with increasing load. The two predicted load-displacement curves diverge slowly before panel buckling, then more rapidly as the load increases, demonstrating the increasing effect of material nonlinearity on the panel response. Good correlation is observed in the figure between the

measured and predicted deflections for $S_{6666} = 4 \times 10^{-14}$ $(lb/in^2)^{-3}$, with a difference between measured and predicted normal deflections of 13 percent RMS. Panel normal deflection contours predicted using that same value of S_{6666} are shown in Figure 9 at an end shortening of 0.130 inches. These contours appear more circular near the panel center, and as square contours with rounded corners towards the edges of the panel.

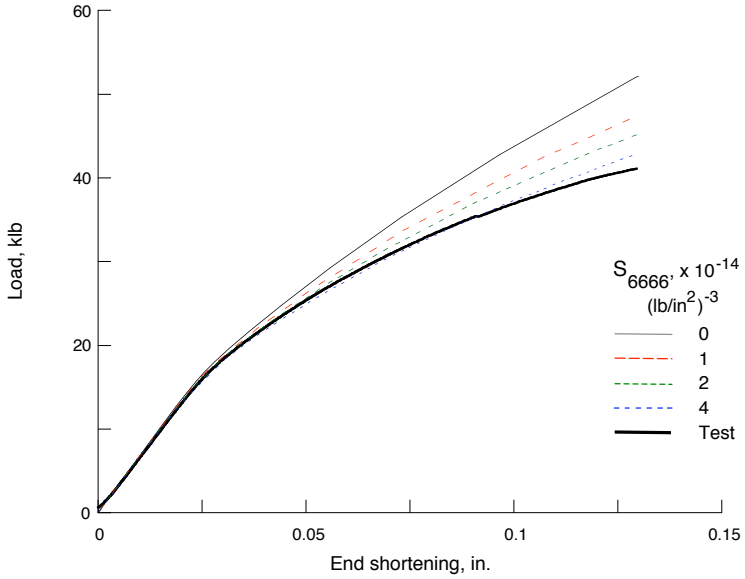

Figure 7. Load vs. end shortening for panel with overlaps

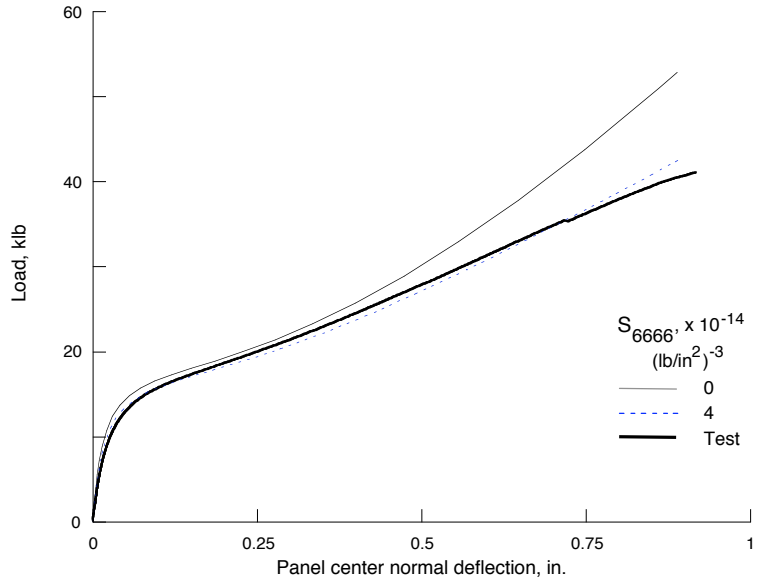

Figure 8. Load vs. panel center normal deflection for panel with overlaps

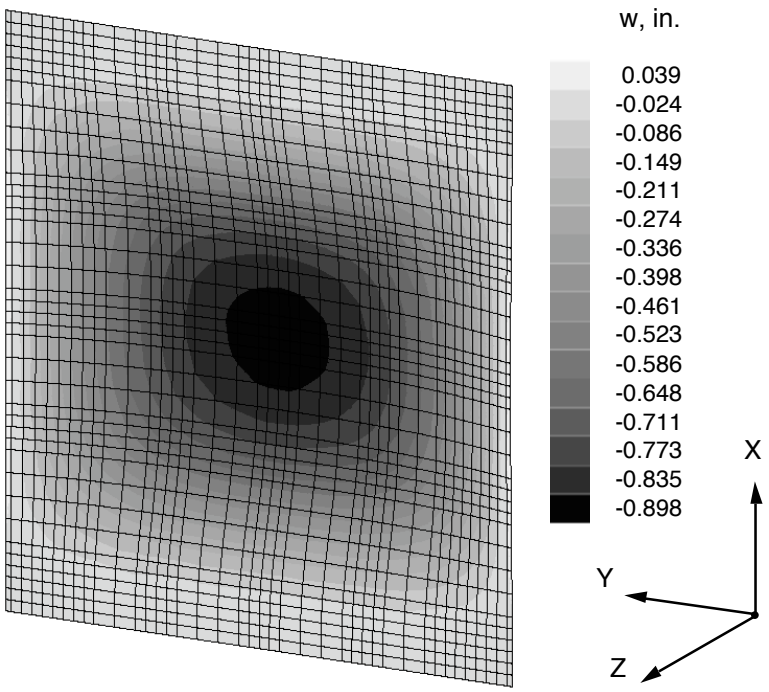

Figure 9. Predicted normal deflection contours for panel with overlaps

Axial and transverse strains

Predicted axial and transverse surface strains from a nonlinear analysis that includes mechanical prestresses and $S_{6666} = 4 \times 10^{-14}$ $(lb/in^2)^{-3}$ are plotted with axial load in Figure 10 at the panel with overlaps center. Also shown in the figure are the measured strain data from the panel test in Ref. 8. Note that compressive strains are negative here. Very good correlation is observed between the measured and predicted strains up to panel buckling, matching the agreement in prebuckling stiffnesses. Although qualitatively similar, the quantitative differences increase in postbuckling, and range from 15 to 42 percent RMS overall. The qualitative correlation between measured and predicted strain data at the other eleven gage locations on the panel with overlaps is assessed as good to excellent.

Predicted axial membrane strains (defined as the average of the front and back surface strains) along the panel transverse centerline are plotted in Figure 11 at applied strains (defined as the average end shortening divided by the nominal 26-inch panel length) of 0.059, 0.132, 0.257 and 0.461 percent. These applied strains correspond to measured axial loads of 10, 20, 30 and 40 klb, respectively. Axial membrane strains measured at those load levels are also plotted for comparison. Good agreement between analysis and experiment is observed across the panel width at both 0.059 and 0.132 percent applied strain, with differences of 13 and 16 percent RMS. Good qualitative correlation is also noted at the higher applied strain levels, but a quantitative comparison shows differences of 28 and 46 percent RMS. The best overall agreement between measured and predicted strains is achieved at gage location 11 near the right-hand simply supported panel edge, with a difference of 8 percent RMS over the plotted load range.

The panel with overlaps analysis with nonlinear material response also gives highly accurate predictions of the resulting axial load at a given applied strain. The analysis predicts a load of 10.23 klb at 0.059 percent applied strain, which is within 2.3 percent of the actual 10 klb load. The difference between the predicted load of 41.10 klb and the measured 40 klb load at 0.461 percent applied strain is 2.7 percent.

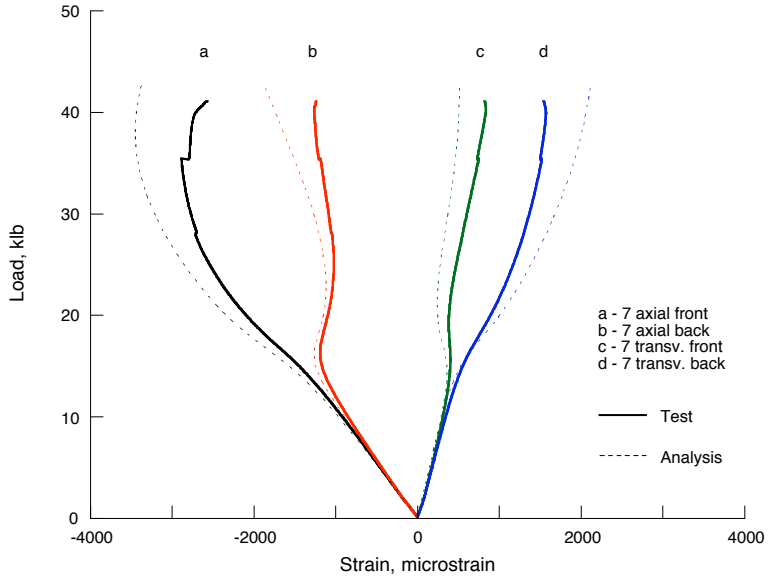

Figure 10. Load vs. strain at gage location 7 for panel with overlaps

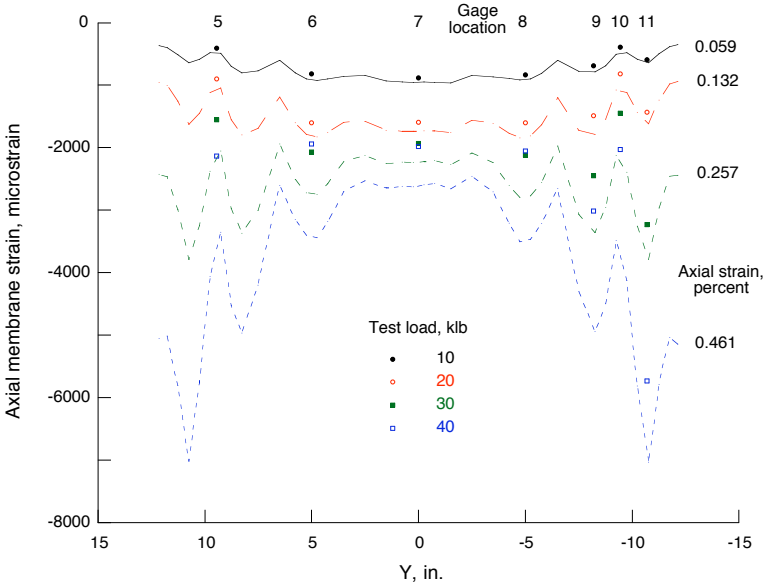

Figure 11. Transverse centerline axial membrane strains for panel with overlaps

Panel without overlaps

The structural response of the panel without overlaps with a nonlinear material model under uniform end shortening is predicted and compared to test results from Ref. 8. The 20-ply laminate thickness of this model is set equal to the average measured panel thickness of 0.149 inches from Ref. 7. While the laminate thicknesses are all assumed to be uniform here, each element still has a unique layup. The fiber orientation angles for the first variable stiffness ply of this model are shown in Figure 12, and provide a good discretization of the continuous fiber orientation angles. However, tow drops (resin-rich pockets located within the variable stiffness ply between successive passes of the tow placement system) resulting from the panel manufacturing process are not modeled here.

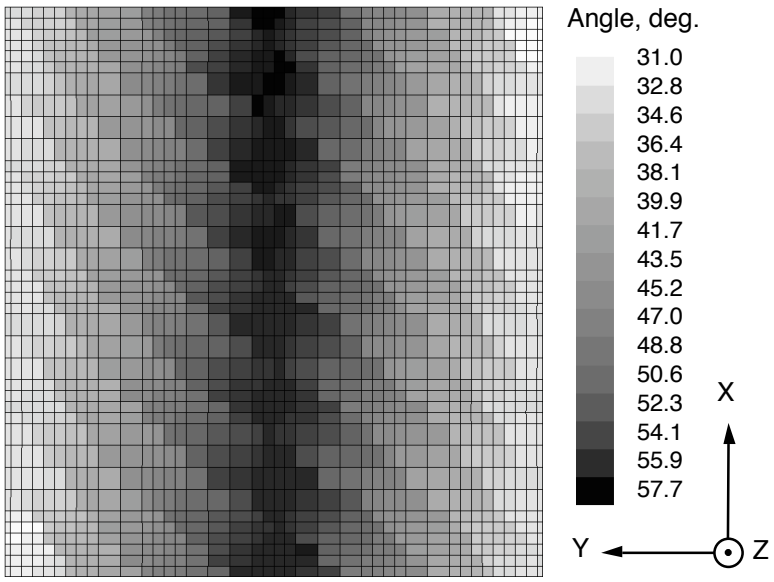

Figure 12. Fiber orientation angles for panel without overlaps analysis model

Axial and normal deflections

The response of the panel without overlaps finite element model including both mechanical prestresses and a nonlinear material model is evaluated for applied end shortenings up to 0.163 inches, the maximum value measured at global failure. The predicted axial load is plotted against the end shortening in Figure 13 for several integer values of the nonlinear parameter S_{6666}, along with the test data (shown as a thick solid line) from Ref. 8. At each end shortening increment with an axial load in excess of 1500 lb, the measured and predicted axial loads are compared. *Predicted forces from a nonlinear analysis with* $S_{6666} = 5 \times 10^{-14}$ *(lb/in*^{2}*)*$^{-3}$ *show very good correlation with the measured results.* A significant local failure occurred at an end shortening of 0.143 inches, as indicated by the discontinuity in the measured load-end shortening curve. Even including this discontinuity, the difference between the experimental and predicted loads is only 1.9 percent RMS.

The predicted prebuckling axial stiffness K_o and the transition load P_{tr} for the panel without overlaps are computed from the load-end shortening curve with $S_{6666} = 5 \times 10^{-14}$ (lb/in^2)$^{-3}$ and shown in Table 1. The analytical prebuckling stiffness of 540.82 klb/in. is within 1.1 percent of the measured stiffness reported in Ref. 8. The predicted transition load is 8.39 klb, or a 9.1 percent difference from the measured transition load. The predicted axial load at the maximum applied displacement is 29.95 klb for this panel, which is a 6.3 percent difference when compared with the measured failure load of 28.13 klb.

Measured and predicted panel center normal deflections are plotted in Figure 14 for the panel without overlaps with $S_{6666} = 0$ and 5×10^{-14} (lb/in^2)$^{-3}$. The two predicted displacement curves compare well up through panel buckling, and then diverge as the load increases. Very good qualitative correlation is observed between the test data and the predicted response for $S_{6666} = 5 \times 10^{-14}$ (lb/in^2)$^{-3}$ up until the discontinuity in the measured results just before global failure. The difference between measured and predicted normal deflections is 25 percent RMS for end shortenings beyond the initial nonlinearity. Predicted normal deflection contours from the analysis with material nonlinearity, shown in Figure 15 at 0.163 inches end shortening, appear more rectangular near the panel center than the contours predicted for the panel with overlaps.

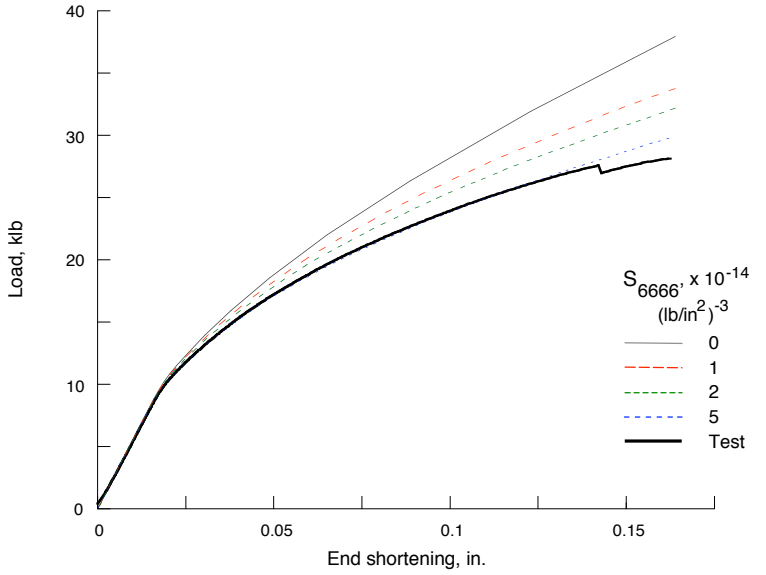

Figure 13. Load vs. end shortening for panel without overlaps

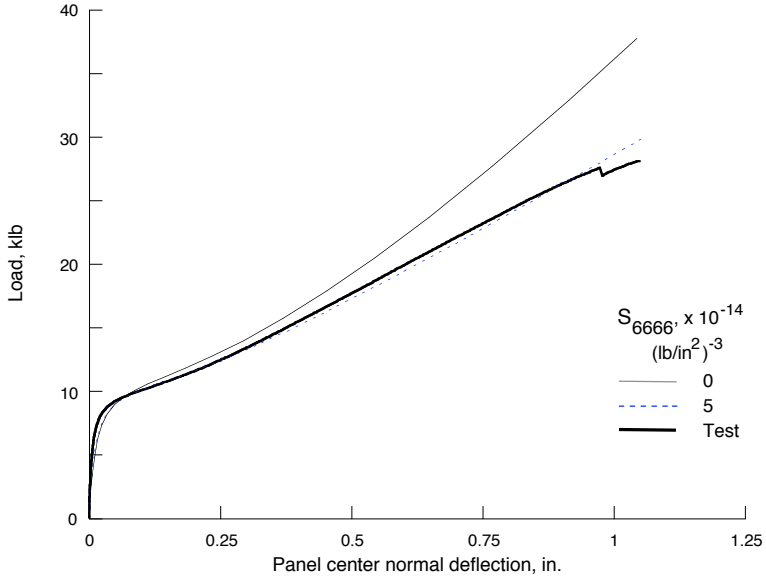

Figure 14. Load vs. panel center normal deflection for panel without overlaps

Axial and transverse strains

Measured and predicted surface strains at the center of the panel without overlaps are plotted against the corresponding axial load in Figure 16. The analysis results include effects of the mechanical prestresses and the nonlinear material response for $S_{6666} = 5 \times 10^{-14}$ $(lb/in^2)^{-3}$. As for the panel with overlaps, the quantitative correlation of strains is excellent up through panel buckling, and then degrades with increasing load. The differences between the measured and predicted strains range from 10 to 37 percent RMS. Evidence of the local panel failure near the maximum applied end shortening is also reflected in discontinuities in the plotted strains. Qualitative comparisons of the test and analysis results range from fair to excellent at the other nine gage locations on this panel.

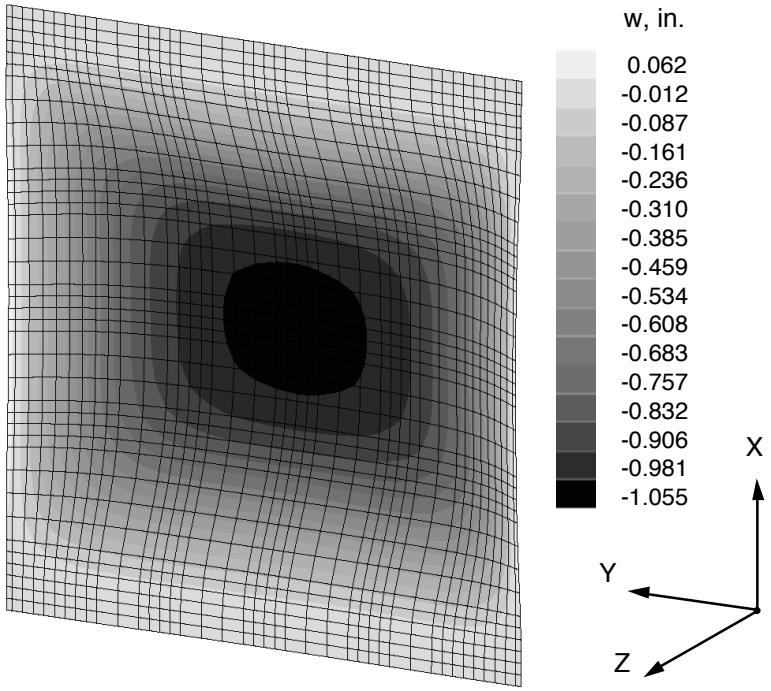

Figure 15. Predicted normal deflection contours for panel without overlaps

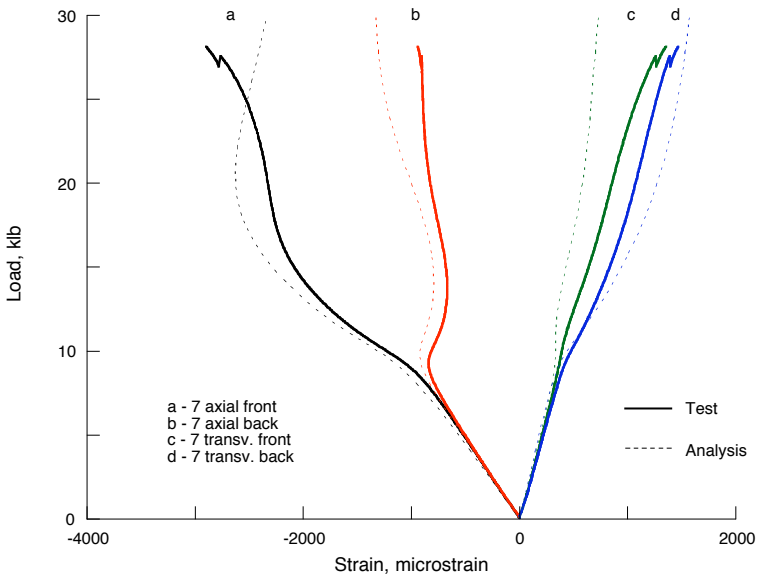

Figure 16. Load vs. strain at gage location 7 for panel without overlaps

Predicted axial membrane strains along the panel transverse centerline are plotted in Figure 17 at 0.036, 0.074, 0.148, 0.261 and 0.425 percent applied strains. These applied strains correspond to measured axial loads of 5, 10, 15, 20 and 25 klb. Axial membrane strains measured at these loads are also shown for comparison. Correlation between the analysis and test results ranges from very good to excellent at the two lowest applied strain levels, with differences of about 9 percent RMS. A qualitative comparison of the membrane strains at the three higher applied strain levels ranges from very good to good along the axial centerline and near the simply supported panel edges to fair at the two gage locations on either side of the axial centerline, with computed differences between 14 and 34 percent RMS.

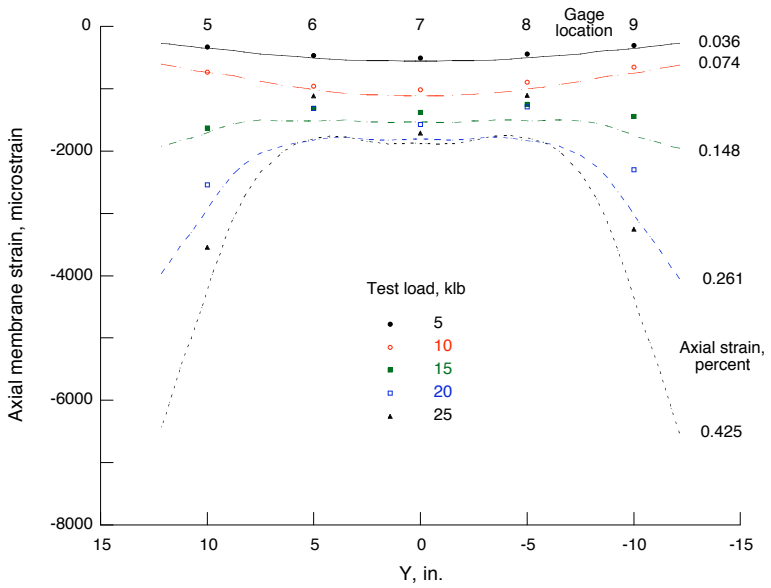

Figure 17. Transverse centerline axial membrane strains for panel without overlaps

The analysis of the panel without overlaps with nonlinear material response again yields accurate predictions of the axial load at any given applied strain. The analysis predicts a load of 5.12 klb at 0.036 percent applied strain, which is 2.4 percent lower than the measured 5 klb load. Near panel failure, the predicted load of 24.96 klb at 0.425 percent applied strain is within 0.2 percent of the actual 25 klb load.

Baseline panel

A finite element model of the baseline panel with a $[\pm 45]_{5S}$ layup is generated in STAGS. A 0.153-inch laminate thickness (equal to the average measured thickness of the baseline panel reported in Ref. 7) is assigned to each element in this analysis model. A mechanical prestress analysis is not performed for this panel because the cured geometric imperfections are very small when compared to the variable stiffness panels. However, measured geometric imperfections for the baseline panel in its structural test fixtures are used for these analyses.

Results from structural analyses of the baseline panel including geometric and material nonlinearities are compared with measurements taken during a baseline panel test to 0.252 inches applied end shortening, at which point the axial displacement transducers reached their limits and the test was terminated. This experiment is designated as the high-load test of the baseline panel to distinguish it from the test results presented in Ref. 8.

Axial and normal deflections

Results from the baseline panel analyses with nonlinear material behavior are presented here. Figure 18 shows a comparison of the axial load-end shortening response of the baseline panel model for several integer values of S_{6666}. The measured response from a high-load test of the baseline panel is also plotted as a thick solid line. For axial loads in excess of the initial test nonlinearity, measured and predicted values are compared at each corresponding value of the end shortening. While the measured responses differ at low loads, *the predicted response for* $S_{6666} = 2 \times 10^{-14}$ *(lb/in*^{2}*)*$^{-3}$ *shows good correlation with the test data for this panel*, with a difference between measured and predicted loads of 10 percent RMS.

The predicted load-end shortening curve with $S_{6666} = 2 \times 10^{-14}$ $(lb/in^2)^{-3}$ is then evaluated to determine the prebuckling axial stiffness K_o and transition load P_{tr}. These values are compared in Table 1 with corresponding results from the high-load test in Figure 18. The difference between the predicted prebuckling stiffness of 502.57 klb/in. and the measured panel axial stiffness is 25 percent, with a 26 percent difference between the predicted transition load of 3.69 klb and the measured value. Differences between the high-load test results presented here and the test data in Ref. 8 are likely due to changes in the material and boundary conditions from additional tests performed on the baseline panel. The predicted axial load of 25.66 klb at the maximum applied displacement of 0.252 inches is within 0.8 percent of the 25.46 klb maximum load recorded during the high-load test.

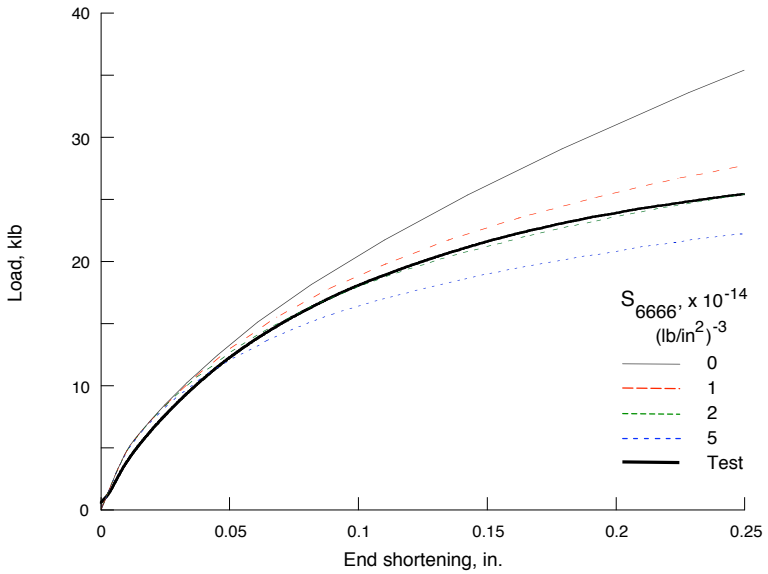

Figure 18. Load vs. end shortening for baseline panel

Baseline panel center normal deflections predicted from analyses with $S_{6666} = 0$ and 2×10^{-14} $(lb/in^2)^{-3}$ are plotted against the corresponding axial load in Figure 19. The analytical load-displacement curves match well up to about 10 klb, but then diverge as the load increases. Measured data from the high-load test are also included for comparison. Good agreement is observed between the analysis results with $S_{6666} = 2 \times 10^{-14}$ $(lb/in^2)^{-3}$ and the test data above 10 klb in the postbuckling load region, up to when the panel center displacement transducer exceeds its linear operating range at approximately 23 klb. The difference in normal deflections over the full range of end shortenings is 14 percent RMS. Predicted normal deflection contours from this analysis, shown in Figure 20, are more elongated in the transverse direction than the variable stiffness panel contours.

Axial and transverse strains

Predicted strains at the panel center from an analysis with $S_{6666} = 2 \times 10^{-14}$ $(lb/in^2)^{-3}$ are plotted in Figure 21 with measured strains from the high-load test. These results compare reasonably well on a qualitative basis, but quantitative correlation ranges from fair to poor because of the highly nonlinear initial strains measured in the high-load test. Differences between the measured and predicted strains range from 24 percent RMS for the front axial gage to 1715 percent RMS for the back axial gage, while correlation for the transverse gages ranges from 36 to 109 percent RMS. Qualitative comparisons of the measured and predicted strains range from fair to very good at the other nine gage locations.

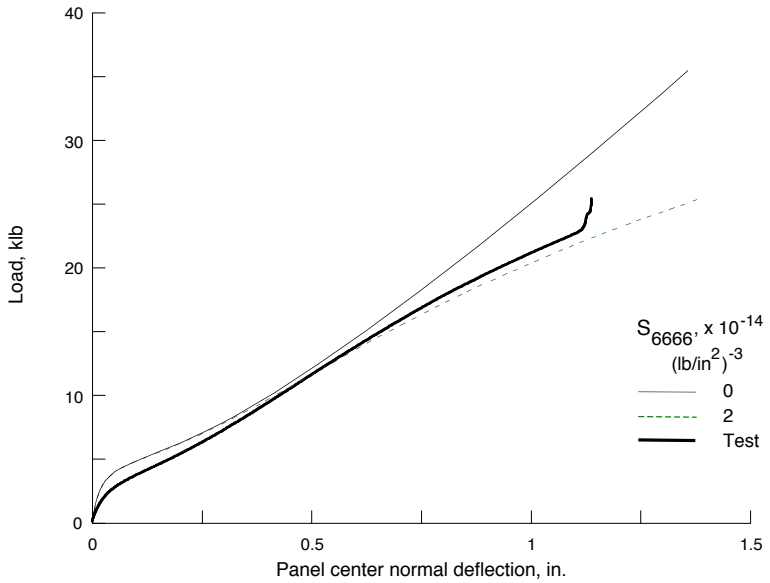

Figure 19. Load vs. panel center normal deflection for baseline panel

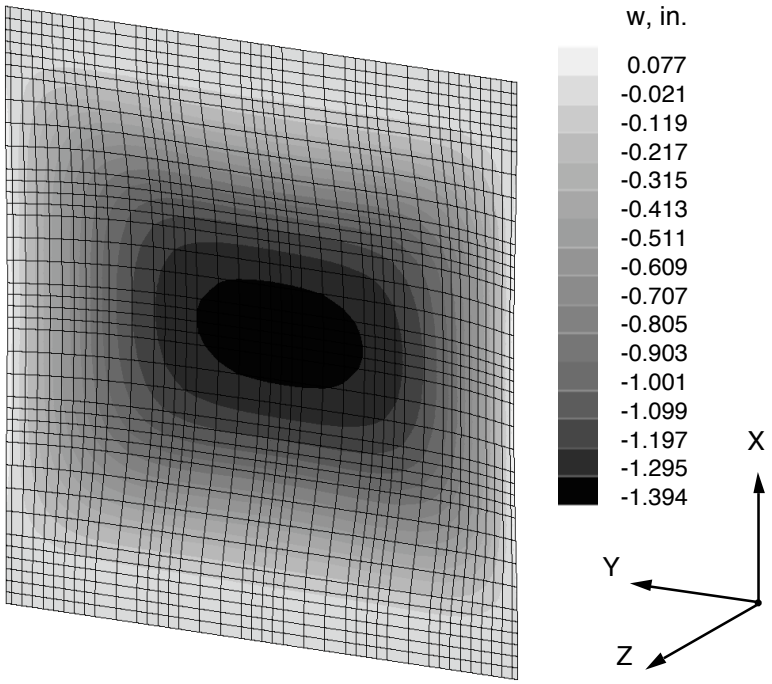

Figure 20. Predicted normal deflection contours for baseline panel

Predicted axial membrane strains along the panel transverse centerline at 0.054, 0.152, 0.270, 0.481 and 0.901 percent applied strains (corresponding to measured axial loads of 5, 10, 15, 20 and 25 klb) are plotted in Figure 22. Measured axial membrane strains at those load levels are also plotted for comparison with the analysis results. Correlation of analysis and test results in the figure ranges from 21 to 35 percent RMS across the range of applied strains. The results shown are qualitatively similar to the corresponding plot for the panel without overlaps, but the peak strain amplitude is approximately two times higher here.

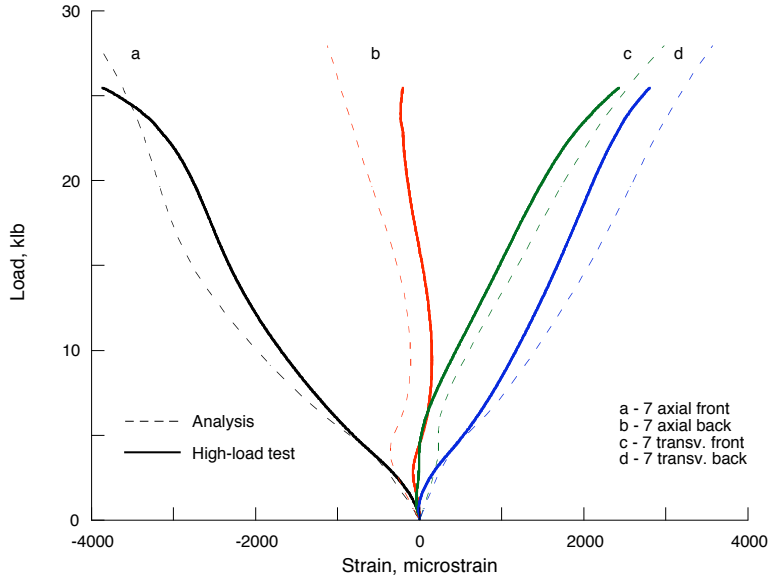

Figure 21. Load vs. strain at gage location 7 for baseline panel

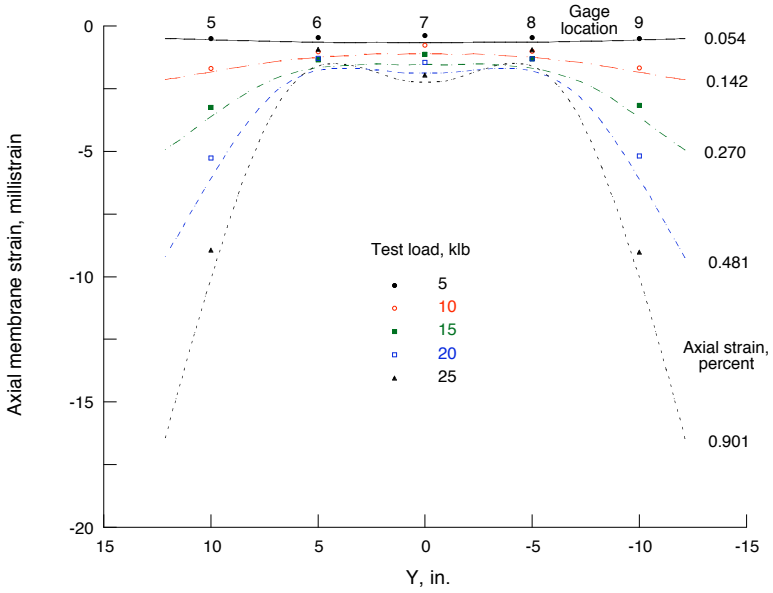

Figure 22. Transverse centerline axial membrane strains for baseline panel

The geometrically nonlinear analysis with nonlinear material response provides accurate predictions of the axial load at higher applied strain levels. The present analysis predicts a load of 5.90 klb at 0.054 percent applied strain, a 17 percent difference from the measured 5 klb load. Near the end of the high-load test, the predicted axial load of 25.04 klb at 0.901 percent applied strain is within 0.2 percent of the measured load of 25 klb.

Concluding remarks

The STAGS analysis code is used to evaluate the structural performance of variable stiffness and baseline panels including both geometric and material nonlinearities. Good correlation between

experiments and analyses is demonstrated for the variable stiffness and baseline panels. The results presented here and in Ref. 8 indicate that an assumption of linear material response is sufficient for prebuckling and near-postbuckling analyses. *However, nonlinear material behavior is an increasingly critical part of the structural response for these panels during deep postbuckling and up to global failure*.

It is difficult (if not impossible) to select an *a priori* value of the nonlinear shear parameter S_{6666} for design purposes. However, reasonable values of S_{6666} may be estimated from analyses of material characterization tests. Analytical studies that include the nonlinear material behavior can then be performed to predict the structural response trends parametrically, and later matched to experimental data from material characterization and structural tests. The analyses performed here show that values of S_{6666} between 0 and 2 x 10^{-14} $(lb/in^2)^{-3}$ show good correlation with the material characterization tests performed on two orthotropic laminates, and values between 2 and 5 x 10^{-14} $(lb/in^2)^{-3}$ result in good correlation for the variable stiffness and baseline panels under end compression loads.

Further correlation of analytical and experimental results would require through characterization of the AS4/977-3 material system in all directions, including determination of failure stresses and strains in tension, compression and shear. This would also allow failure predictions to be made using the progressive failure analysis capability in STAGS. A material model that includes the nonlinear transverse response of a composite ply would also be desirable, although that effect will most likely be small compared to that of the nonlinear shear behavior demonstrated here for these composite panels.

References

1. Evans, D. O., Vaniglia, M. M., and Hopkins, P. C.; *Fiber Placement Process Study*. Proceedings of the 34th International SAMPE Symposium, Vol. 34, Book 2, May 1989, pp. 1822-1833.
2. Gürdal, Z., and Olmedo, R.; *In-Plane Response of Laminates with Spatially Varying Fiber Orientations: Variable Stiffness Concept*. AIAA Journal, Vol. 31, No. 4, April 1993, pp. 751-758.
3. Olmedo, R., and Gürdal, Z.; *Buckling Response of Laminates with Spatially Varying Fiber Orientations*. Proceedings of the 34th AIAA/ ASME/ASCE/AHS/ASC Structures, Structural Dynamics, and Materials Conference, April 19-21, 1993, La Jolla, CA, pp. 2261-2269. Paper No. AIAA 93-1567.
4. Waldhart, C., Gürdal, Z., and Ribbens, C.; *Analysis of Tow-Placed, Parallel Fiber, Variable Stiffness Laminates*. Proceedings of the 37th AIAA/ASME/ASCE/AHS/ASC Structures, Structural Dynamics, and Materials Conference, April 15-17, 1996, Salt Lake City, UT. Paper No. AIAA 96-1569.
5. Langley, P. T.; *Finite Element Modeling of Tow-Placed Variable-Stiffness Composite Laminates*. M. S. Thesis, Virginia Polytechnic Institute and State University, 1999.
6. Tatting B. F., and Gürdal, Z.; *Design and Manufacture of Tow-Placed Variable Stiffness Composite Laminates with Manufacturing Considerations*. Proceedings of 13th U.S. National Congress of Applied Mechanics, June 21-26, 1998, Gainesville, FL.
7. Wu, K. C. and Gürdal, Z.; *Thermal Testing of Tow-Placed, Variable Stiffness Panels*. Proceedings of the 42nd AIAA/ASME/ASCE/AHS/ASC Structures, Structural Dynamics and Materials Conference, Seattle, WA, April 16-19, 2001. Paper No. AIAA 2001-1190.
8. Wu, K. C., Gürdal, Z. and Starnes, J. H., Jr.; *Structural Response of Compression-Loaded, Tow-Placed, Variable Stiffness Panels*. Proceedings of the 43rd AIAA/ASME/ASCE/AHS/ASC Structures, Structural Dynamics and Materials Conference, Denver, CO, April 22-25, 2002. Paper No. AIAA 2002-1512.
9. Peel, L. D., Hyer, M. W. and Shuart, M. J.; *Compression Failure of Angle-Ply Laminates*. NASA CR-189485, September 1991.
10. Hahn, H. T. and Tsai, S. W.; *Nonlinear Elastic Behavior of Unidirectional Composite Laminae*. Journal of Composite Materials, Vol. 7, No. 1, January 1973, pp. 102-118.
11. Rankin, C. C., et al.; *STAGS User Manual, Version 5.0*. Lockheed Martin Missiles & Space Co., Inc., Palo Alto, CA, December 2003.

Tables

Table 1: Predicted performance for variable stiffness and baseline panels.
Analyses with measured imperfections and geometric and material nonlinearity.

Prestress case	Panel with overlaps		Panel without overlaps		Baseline panel	
	K_o, klb/in	P_{tr}, klb	K_o, klb/in	P_{tr}, klb	K_o, klb/in	P_{tr}, klb
None	–	–	–	–	502.57	3.69
Mechanical	664.30	12.39	540.82	8.39	–	–
Test	649.86	13.64	534.76	9.19	392.39	2.83